



## First results of the refurbished SOUSY radar: Tropopause altitude climatology at 78°N, 16°E, 2008

C. M. Hall,<sup>1</sup> J. Röttger,<sup>2</sup> K. Kuyeng,<sup>3</sup> F. Sigernes,<sup>4</sup> S. Claes,<sup>4</sup> and J. Chau<sup>3</sup>

Received 15 January 2009; revised 19 June 2009; accepted 15 July 2009; published 30 September 2009.

[1] The second generation SOUSY MST radar at 78°N, 16°E on Svalbard has recently completed its inaugural year of combined troposphere and mesosphere observations. Here, troposphere observations have been processed using a robust detection algorithm designed for obtaining tropopause climatology by automatic data processing, and the resulting monthly statistics have been compared with corresponding surface air temperatures. As our main objective, we describe the new radar system, present the tropopause detection method, and validate the results using radiosonde and surface temperature data. The tropopause height depends on the temperature of the underlying atmosphere but is also influenced by downward control from the stratosphere. We find that the climatological tropopause height is correlated with the surface temperature but with the former lagging the latter by approximately 1 month.

**Citation:** Hall, C. M., J. Röttger, K. Kuyeng, F. Sigernes, S. Claes, and J. Chau (2009), First results of the refurbished SOUSY radar: Tropopause altitude climatology at 78°N, 16°E, 2008, *Radio Sci.*, 44, RS5008, doi:10.1029/2009RS004144.

### 1. Introduction and the SSR2 Radar

[2] The SOUSY Svalbard Radar (SSR2) is located in Adventdalen on Svalbard at 78°N, 16°E, in close proximity to two field stations operated by The University Centre in Svalbard (UNIS) providing, inter alia, meteorological data and close to the EISCAT Svalbard Radar. Since SSR2 is a relatively new installation, is innovative and not yet fully documented, we shall begin with a description of the system. The original SOUSY radar on Svalbard [Röttger, 2001a, 2001b] was designed to operate with a typical peak power of more than 60 kW and transmitting in steerable beams in five directions including the zenith, achieved through a phased array of 356 four-element Yagis. Owing to the relatively high transmitter power (requiring operators to be present), operation was normally limited to a campaign basis, but by using only the 4 kW driver stage and not the final amplifier, it was possible to achieve unattended operation. Because of the system design, however, operator intervention was often required and, due to an aging tech-

nology, it was decided to improve reliability at the cost of flexibility and power, work being completed in late summer 2007. The refurbished system, SSR2, still uses the original antenna array, although without beam steering; only a vertical beam is used, this having a half power full width of 5°. Owing to damage by excessive snow drift, some of the Yagi elements were partly damaged. We estimate that this reduces the total antenna gain by less than 3 dB. The transmitter has been replaced by a 1 kW peak (and 10% duty cycle) solid state unit supplied by Vikas (India) operating at 53.5 MHz and a second unit is currently available to either double the power or to provide redundancy. The other major improvements to the SSR2 radar are the radar controller and acquisition system, based on digital receiver design, which have been developed at Jicamarca Radio Observatory (JRO) where a similar system is used as the main acquisition system of the radars there. The block diagram of the system is shown in Figure 1 in which gray boxes are components designed and built at JRO.

[3] The main components of the new radar control and data acquisition system are:

[4] 1. The radar controller, based on CPLD (complex programmable logic device), controls the transmitting and receiving part. It has eight control lines, TTL output level, and is programmed with a PC through a serial cable using the program “PulseDesign.” This software, developed at JRO, facilitates the creation of radar experiments with its graphical user interface and also includes the parameters for acquisition system and online process.

<sup>1</sup>Tromsø Geophysical Observatory, University of Tromsø, Tromsø, Norway.

<sup>2</sup>Max Planck Institute, Katlenburg-Lindau, Germany.

<sup>3</sup>Radio Observatorio de Jicamarca, Instituto Geofísico del Perú, Lima, Peru.

<sup>4</sup>University Centre in Svalbard, Longyearbyen, Norway.

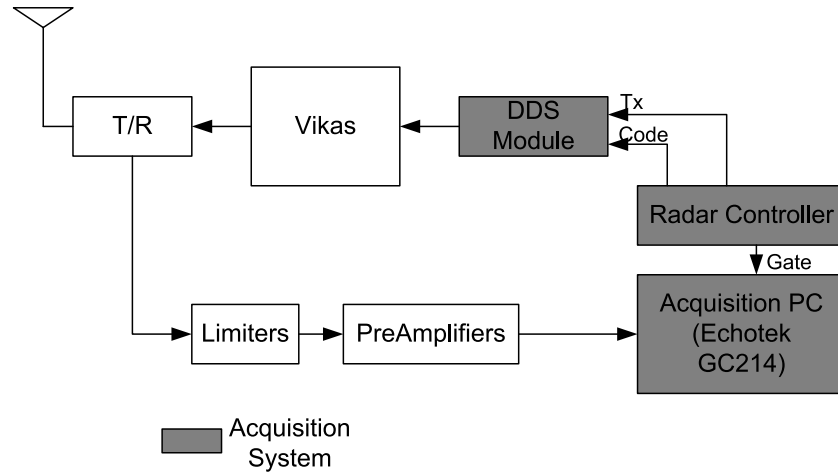


**Figure 1.** Block diagram of the SSR2 system. Gray boxes are those components designed and built by Jicamarca Radio Observatory. “T/R” is a passive transmit-receive switch (manufactured by Max Planck Institute, Germany); “Vikas” is the actual transmitter (built by Vikas, India); DDS is the acronym for “direct digital synthesis” and generates waveforms for the transmitter.

[5] 2. The DDS (direct digital synthesis) Module, based on an AD9854 card, generates the pulsed/coded RF for the transmitter. The frequency and pulse trains are programmed with a PC through the parallel port sending a file generated with the AD9854/52 software from the manufacturer.

[6] 3. The Acquisition PC is the digital receiver used for this acquisition system and is an Echotek GC214-PCI board installed on the PCI port on the PC. The software has been developed at JRO that not only programs the card and acquires the data but performs online process like coherent integrations, decoding and also FFT to save spectra; for online system checks sample sets of raw data can be made available as well.

[7] All components can be controlled over the Internet but normally the system runs without any intervention whatsoever. The normal mode of operation is one of 20-min cycles of 10 min troposphere–lower stratosphere (ST) followed by 10 min mesosphere (M) soundings and this resulting data set is unprecedented for this geographic location. An improvement is planned to shorten this relatively long interlace time of 20 min to a fraction of a second by changing between these M and ST modes after each coherent integration period. Furthermore, the price tag has been exceptionally low, excepting the antenna array which is part of the original SOUSY installation on Svalbard. For the study discussed here, the troposphere–lower stratosphere data were taken with 1 kW peak power, a duty cycle of 3.3%, and a 4-bit complementary code with 150 m resolution.

[8] The current system can typically detect tropospheric echoes from 4km to the radar-tropopause altitude

(discussed in detail later). In the intervening region, features generating sufficient gradients in refractive index to provide radar echoes include turbulence, gravity waves, fronts, tropopause folding and multiple tropopauses as described by Röttger [2001a] from experience with SSR1. From the quasi-simultaneous mesosphere soundings, Polar Mesospheric Summer Echoes (PMSE) [e.g., Röttger, 2000] are observed and meteors have also been detected around 90 km altitude.

## 2. Tropopause Detection

[9] From the different definitions of the tropopause height we have chosen the most standard one, viz. that the tropopause is defined as the altitude at which the temperature structure of the lower atmosphere ceases to be characterized by the saturated adiabatic lapse rate [e.g., Salby, 1996; *World Meteorological Organization (WMO)*, 1996]. The actual measurement of the tropopause height, however has given rise to a number of other definitions depending on the measurement technique, as discussed by, for example, Hooper and Arvelius [2000]. Radar-based methods include those by Gage and Green [1979, 1982]. In this study we shall simply use echo return power as was the approach of Röttger and Hall [2007], and thus hereafter the term “tropopause” may be read as “radar tropopause.” While our data analysis method, while essentially based on Gage and Green [1982], is innovative (not least using first results from a new instrument, as described above) the resulting statistics complement those from the study by Röttger and Hall [2007] using the old SOUSY system at the same location.

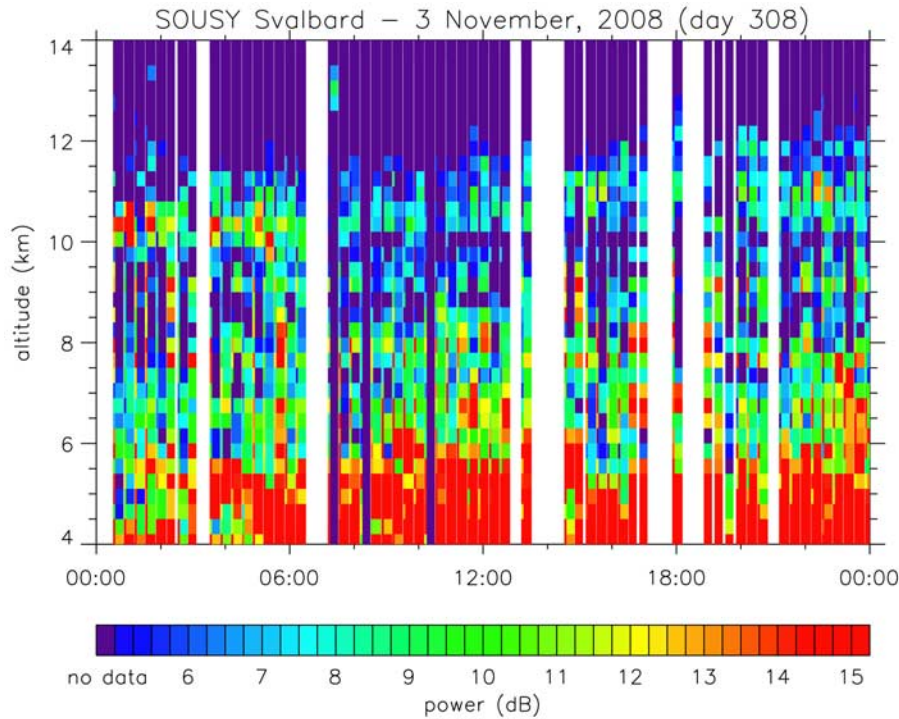


**Figure 2.** Typical day of tropospheric soundings. White stripes indicate missing data.

While *Röttger and Hall* [2007] digitized range-time-intensity plots of radar returns by eye, such methods are prone to subjectivity; in order to process data from the new SOUSY system we have sought an automatic method. Such algorithms are still bound by the subjectivity of the programmer, but thereafter the same rules are applied regardless of both the data quality and real atmospheric structure. We have tested the method of *Hooper and Arvelius* [2000] but found it to perform poorly on our data, not due to inadequacy of the algorithm, but rather the noisy and occasionally intermittent nature of the SOUSY data. The tropospheric–lower stratospheric data flow can be interrupted by mesosphere observations, inhibited transmission due to local Air Traffic Control, temporary system failure etc., and furthermore, detection problems can arise from tropopause weakening (i.e., a reduction of the temperature gradient above the tropopause, as we discuss later), disappearance, multiple tropopauses, fronts and folding [cf. *Röttger*, 2001a].

[10] Figure 2 shows a typical day of tropopause soundings of the SSR2. In the lower regions of this plot, we can see large echo returns due to enhanced reflectivity, likely by reflectivity enhanced by humidity gradients in convective turbulence and some degree of wave structure (seen by, for example, downward propagating wavefronts at 0800–0600 and 1200–1600 UT). Progressing

to greater altitudes, we see a region with little signal followed by the characteristic echo layer, the radar tropopause, caused by the steepened mean refractivity gradient above the tropopause. The radar tropopause itself varies in altitude during the course of the 24 h shown here, and also varies in intensity (as defined by echo power), with underlying layer structures occasionally exhibiting similar echo power. The radar tropopause is 2–3 km above the meteorologically defined tropopause (as we shall see in Figure 5). The effective radar cross section at VHF, regardless of whether the signal is from pure turbulence layers or from specular-type reflectivity sheets, is proportional to the square of the mean gradient of the refractive index; this in turn is proportional to the square of the Brunt-Väisälä frequency which depends linearly on the potential temperature gradient. In effect this directly implies that one expects a maximum in echo power corresponding to the maximum in temperature gradient, this normally occurring in the lower stratosphere, perhaps as much as 3 km [e.g., *Röttger and Hall*, 2007] above the meteorological tropopause defined as the lowest level at which the lapse rate decreases to  $2 \text{ K km}^{-1}$  or less, provided that the average lapse rate between this level and all higher levels within 2 km does not exceed  $2 \text{ K km}^{-1}$ . To confirm the correct operation of the radar, we have obtained temperature profiles from

the micro pulse lidar operated by the National Institute of Polar Research (Japan) in Ny Ålesund (78.9°N, 11.9°E): for 3 November 2008 (as in Figure 2) the maximum temperature gradient occurred at 10.5 km thus corresponding to the echo layer in Figure 2 (we have actually performed several such “spot checks”). On average the displacement of temperature gradient maximum above the temperature minimum is roughly constant and thus we can regard the radar tropopause height variations to replicate those of the meteorological tropopause, as we shall see in the next section.

[11] The online analysis in the radar system typically delivers profiles with a 4 min resolution for the experimental setup used here. Following noise-floor subtraction in the spectral domain [Hildebrand and Sekhon, 1974], we remove short-lived events by applying an erosion algorithm to the signal power time series at each height. We employ a structuring element  $B_1 = \{0, 1, 1, 0\}$  in the time dimension ( $B_1$  is thus a binary vector of length 16 min) which will impose removal of events shorter than 8 min. This operation is one of removal (= erosion) by comparison with the boxcar  $B_1$  as distinct from smoothing. The resulting filtered time series  $C$  is obtained from the original time series  $A$  by:

$$C = A \otimes B_1 = \bigcap_{b \in B} (A)_{-b} \quad (1)$$

where  $(A)_{-b}$  represents the translation of  $A$  by  $b$ . Thereafter each power profile is multiplied by range<sup>2</sup> (in km<sup>2</sup>) (and thus hereafter the power becomes range-corrected power, the absolute values of which need not concern us). This approach is very similar to that of Gage and Green [1982], who defined the tropopause altitudes as where the range-squared corrected power crosses a preset threshold. This is equivalent to detecting where the temperature gradient exceeds a threshold value, in contrast to the method used here wherein the altitude identifies where the corrected power/temperature gradient has its maximum value. Again, the range-squared correction step is purely to enhance the tropopause detectability. We are aware that this formalism also unrealistically enhances any noise power not already removed by subtraction of the noise floor, but it is essential to assure that we trace detectable echoes by means of their reflectivity. Thus, weighted power profiles exhibit enhanced signal with increasing altitude and effectively suppresses any peaks at lower altitudes where refractive index is determined by humidity, but at the same time we have avoided a preconception of where the tropopause might occur. An alternative to range-correcting the power might have been the application of, for example, a Gaussian weighting centered on a guessed tropopause height; this, we feel however, has less physical justification than the

range correction method. Finally, a morphological top-hat operation [e.g., Jackway, 2000] is applied. Here the structuring element is given by

$$B_2 = \begin{Bmatrix} 0 & 0 & 0 & 0 & 0 \\ 1 & 1 & 1 & 1 & 1 \\ 0 & 0 & 0 & 0 & 0 \end{Bmatrix} \quad (2)$$

in which the lengths of the elements are 4 min (giving the top hat a total length of 20 min) and each row of  $B_2$  corresponds to three range gates of 150 m each (the width of the two-dimensional “hat” thus being 450 m with a 150 m “brim” (see illustration of the top-hat morphing operation in the work of Jackway [2000])). In practice, owing to the interleaved mesospheric soundings, this ensures spanning two troposphere sounding periods and giving an average top-hat length of 26 min. The maximum in each hourly mean profile is then identified and registered as a radar tropopause height if it exceeds a threshold corresponding to 10dB prior to applying the range<sup>2</sup> weighting. For the purposes of the interpretation that follows, we deem it better to arrive a null result (i.e., failure to detect an unambiguous maximum power) when echoes are so weak or ambiguous that the radar tropopause is poorly defined rather than an incorrect estimate; nevertheless, isolated erroneous maxima can still be detected, particularly when the radar tropopause is a weak feature and there are strong underlying layers (e.g., due to fronts or folding).

[12] A typical analysis is shown in Figure 3. Here, the background plot shows the eroded, range-corrected/weighted and top-hat morphed data from Figure 2. The cyan line in the plot indicates the hourly maxima. As an illustration only, we have also applied a 5 h median filter to show how individual outliers might be removed. We see that at 0830 UT the radar tropopause as we perceive it from Figure 2 was weak and the detection algorithm has identified a lower layer. This is evidently a pathological case and the median filtering has successfully removed it. The same is not true at the end of the day, but in practice all available days are processed and the median filtering is applied to the entire time series wherein such events are similarly pathological.

[13] The method described above works satisfactorily with the SSR2 experiment it was optimized to analyze. However, change of time and/or height resolutions would likely alter the optimal values for the structuring elements for either or both spike erosion and top-hat morphing. Applying the methodology to other radar data should include some degree of trial-and-error adjustment of these structuring elements: recall that we found that the Hooper and Arvelius [2000] method did not work well on our data. Furthermore it is conceivable that at other

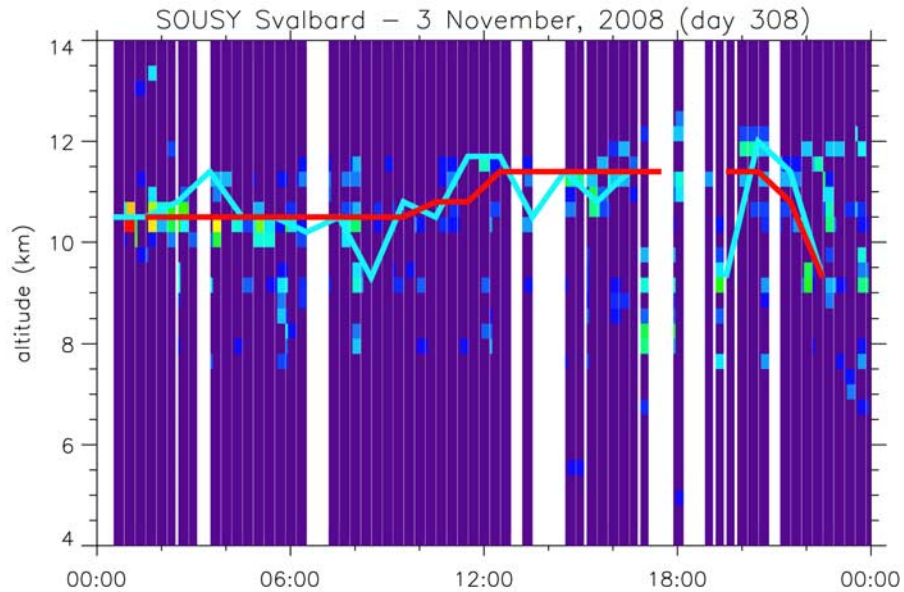


**Figure 3.** Results of tropopause detection for a typical day. The background plot shows the eroded, range-corrected/weighted and top-hat morphed data from Figure 2. The superimposed cyan line indicates the hourly maxima, and the red line shows how individual outliers can be removed with a median filter.

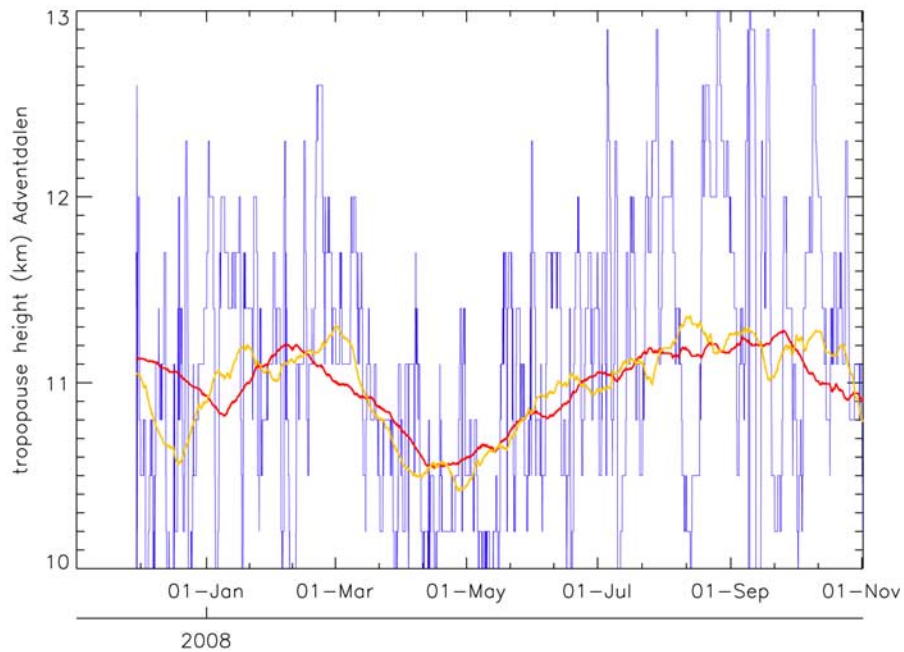


**Figure 4.** Daily tropopause heights (thin blue line) for all available days of SSR2 operation. Superimposed are a 1-month Lee filtered series (red) and 1-month boxcar smoothed series (orange).

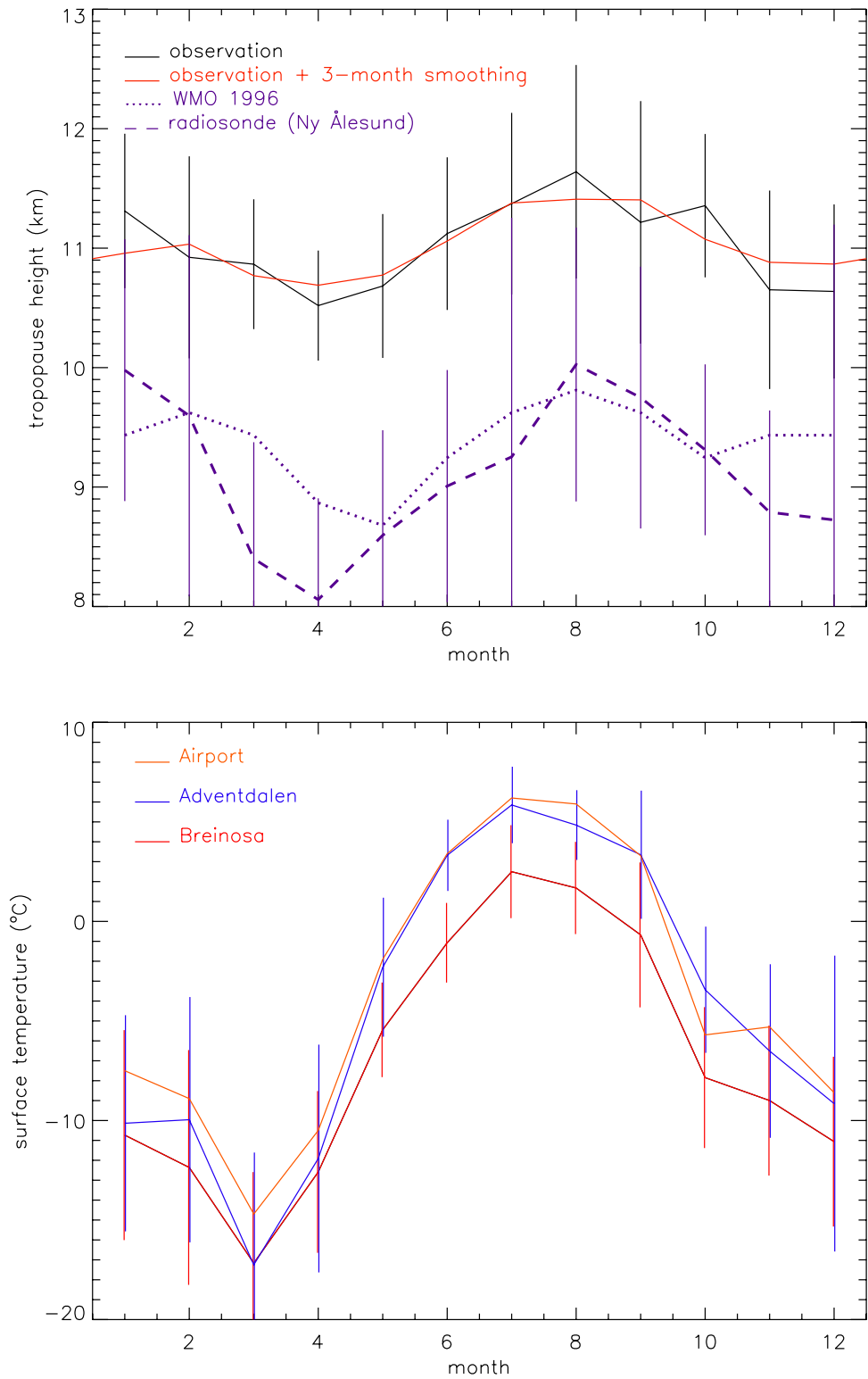


Figure 5

geographic locations the tropopause signal may occupy more (or less) height, may well be at different altitude and be more (or less) separated from the almost ubiquitous turbulence signal in the lower troposphere, thus affecting whether the range<sup>2</sup> or another form of weighting is applied.

### 3. Verification and Interpretation

[14] After applying the detection algorithm for all available days, a 1-day wide median filter can be applied as described and illustrated above. In what follows, we shall not examine tropopause variability at intraday scales, making this filter length appropriate. Taking all available days from the SSR2 operation hitherto, we thus arrive at Figure 4. The aforementioned 1-day running median is portrayed by the thin fluctuating line. As examples of further smoothing, applications of 1-month Lee and boxcar filters are shown by the superimposed red and orange lines respectively. If we then form monthly means we obtain the annual variation shown in Figure 5. Again, as an illustration, we show the result of concatenating the same 12-month time series three times over and smoothing with a 3-month median filter in order to eliminate edge effects. Furthermore, the *WMO* [1996] climatology is included. The latter exhibits a very similar annual variation, the height discrepancy arising from differing definitions of the tropopause (as explained earlier). The de facto validation is, however, via comparison with meteorological tropopause determinations by radiosonde, in this case from Ny Ålesund (Koldewey Station of the Alfred Wegener Institute), again, given as monthly means and standard deviations in Figure 5. The approximately constant displacement of the radar tropopause above the meteorological (radiosonde) tropopause is evident; the seasonal variation is in excellent agreement with the late-winter minima and late summer maxima coinciding exactly. At lag 0 (months) the cross-correlation coefficient maximized at 0.84. In Figure 6, we show the height difference between the radar and radiosonde tropopause monthly means; the difference is greatest in April but the annual variability amounts to only 20%. In Figure 6 (bottom) we show a scatterplot comparing the two sets of measurements and with little spread around the linear regression line. In future work, one could consider using this relationship to derive the meteorological tropopause from the radar observations.

[15] Although the above comparison gives us considerable confidence in the radar tropopause detection algorithm, especially after filtering and averaging (in obtaining monthly means) has removed outliers (whatever their origin), we shall continue the validation of the method by comparing with temperature data. A major, but not sole, factor deciding the tropopause altitude is the mean troposphere temperature, but really only when the temperature profile is characterized by the saturated adiabatic lapse rate. In general, on longer timescales, the tropical tropopause is correlated with the temperature in the upper troposphere and lower stratosphere (or Brewer Dobson circulation). At very high latitude where insolation of the surface is small or, for several months of the year, absent altogether, large inversion layers may exist and convective mixing may be minimal, thus, while the surface temperature is strongly correlated with the tropopause altitude in the tropics [e.g., Reid and Gage, 1981], we should not necessarily expect the same at very high latitude. We have obtained mean surface air temperatures corresponding to the months in Figure 5 (top) from three different close by locations: Longyearbyen airport (approximately 12 km to the NW, courtesy of the Norwegian Meteorological Institute), Adventdalen (approximately 5 km to the NW) and the Kjell Henriksen Observatory at Breinosa (approximately 1 km to the SE but at 520 m above sea level), all shown in Figure 5 (bottom). The first location is adjacent to the sea and may be thought of as a control. Breinosa is nearest to SSR2 but some 500m above it. Adventdalen is at the same altitude as SSR2 and in a valley floor. As seen in Figure 5, the three sets of measurements are in good agreement (Breinosa, due to its greater altitude, being systematically colder as expected). In March, the airport location is warmer presumably due to advection of sea surface air, whereas the Adventdalen and Breinosa temperatures are the same, possibly indicating katabatic flow from the mountain into the valley. Comparing the two panels in Figure 5 we see very similar seasonal variation but with the temperature minimum and maximum leading the tropopause minimum and maximum altitudes by 1 month (the time resolution here is only 1 month). Correlation coefficients for cross correlations between radar tropopause height and surface temperature maximize at a lag of 1 month: 0.72 for Adventdalen and 0.75 for Breinosa. The corresponding cross correlation between meteorological tropopause height from Ny Ålesund

**Figure 5.** (top) Tropopause monthly means for 2007–2008 and standard deviations (black); 3-month median filtered series removing edge effects (red); *WMO* [1996] prediction (dotted); meteorological tropopause from radiosondes from Ny Ålesund (dashed). (Ny-Ålesund radiosonde data from Alfred Wegener Institute, courtesy of M. Maturilli.) (bottom) Monthly mean surface air temperatures from three sites near SSR2 for 2007–2008: Longyearbyen airport (approximately 12 km to the NW, courtesy of the Norwegian Meteorological Institute), Adventdalen (approximately 5 km to the NW), and Breinosa (approximately 1 km to the SE but at 520 m above sea level).

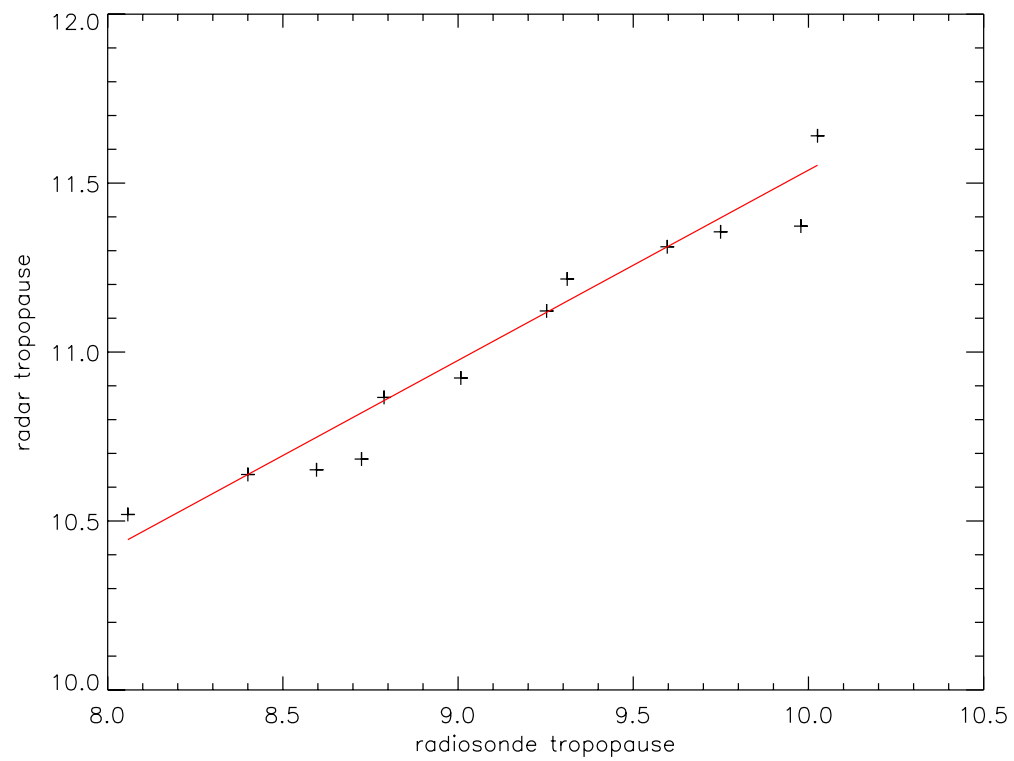
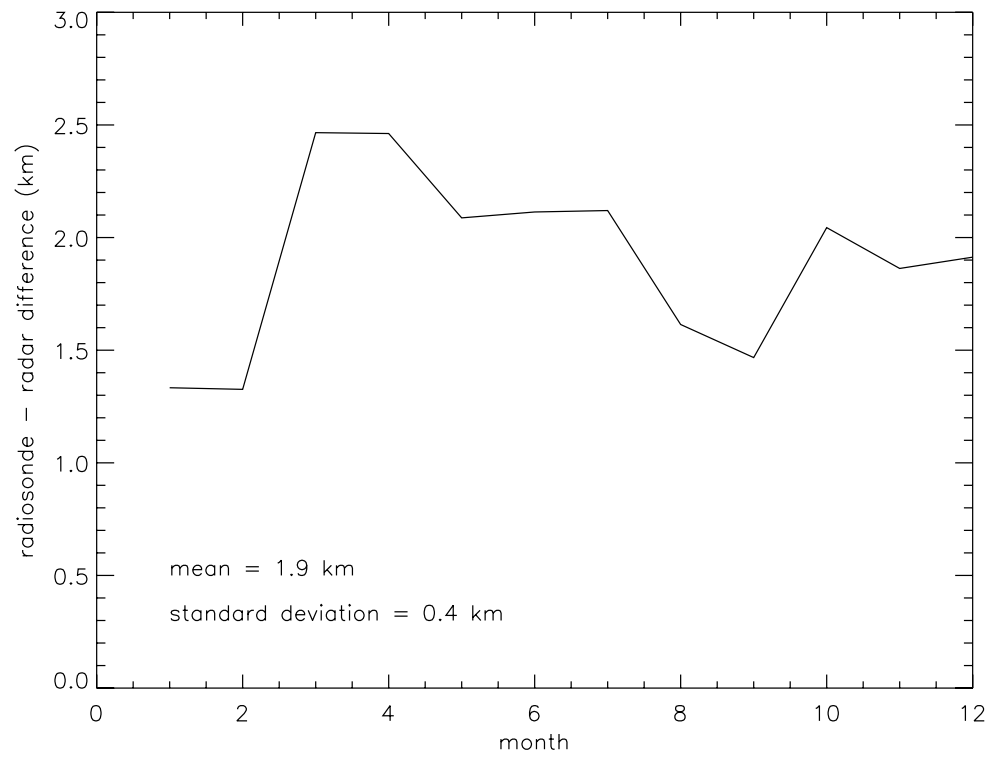


Figure 6



and surface temperatures in Adventdalen is also shown, and exhibiting the same lag.

[16] As a final comparison, we can recall the results of *Röttger and Hall* [2007] obtained using the original SOUSY system (SSR1) at exactly the same geographical location (recall that the antenna array remained unchanged in the upgrade to SSR2 and therefore the fields of view are the same). The results from this study are reproduced in Figure 7 (top). Certainly within the respective standard deviations (which reflect the intramonth variability), the agreement between the 2007–2008 seasonal variation and that from the period 2004–2006 is very good. The Kjell Henriksen Observatory at Breinosa was not built at that time and thus we simply use temperatures from Longyearbyen airport and these monthly means for the years 2004–2006 are shown in Figure 7 (bottom). Although at first glance it may seem these temperature and tropopause height variations are in phase, the cross correlation actually maximizes at a lag of 1 month as before, with a coefficient of 0.78, and, further punctuating this point, a Spearman rank correlation [*Spearman*, 1904] with confidence 98%. All correlation analyses are shown in Figure 8 in which the lag is clearly consistent between all three comparisons. To better investigate the potential correlation and the lag, using single day data, i.e., having a large number of samples for the correlation SSR2/2008 data analysis, yielded a lag of 28 days.

[17] Although the physics of the relationship between surface air temperature and tropopause altitude lies beyond this goal we shall briefly address it here. Night-time boundary layer temperature inversion is a well known phenomenon [e.g., *Salby*, 1996] but at high latitude in winter the effect is particularly strong since, due to continuous darkness and thus less diurnal variation, there is a total lack of surface insolation for several months. This lack of heating further results in reduced convection; indeed, in the absence of convective mixing and synoptic-scale disturbances, and for Newtonian cooling alone the (thus radiative) timescale is of the order of 10 days in the troposphere [*Salby*, 1996] or even double that (extrapolating Figure 8.29 of *Salby* [1996] to the tropopause altitudes we report here). The air temperature at ground level (what we introduced as “surface air temperature”), particularly in winter may well not be representative of the mean temperature of the troposphere, therefore, and it is the latter that, in part, determines the tropopause altitude. Even in summer, the sun’s elevation is small and convective instability is not generally a feature of the atmosphere in polar latitudes, such as on Svalbard. Another factor affecting tropopause height

is downward control from the stratosphere. There is normally a less positive vertical gradient of temperature in the lower stratosphere in winter, but when the polar vortex breaks up ozone rich air is transported poleward into the arctic stratosphere from the south [e.g., *Andrews et al.*, 1987]. Thereafter the return of sunlight in late winter gives rise to ozone heating, increasing of the temperature gradient and subsequent depression of the tropopause. Variability in tropopause height and corresponding variation in stratospheric temperature have been studied in detail previously [e.g., *Angell and Korshover*, 1964; *Reid and Gage*, 1981, 1985]. Furthermore, it should be remembered that large-scale dynamics in polar regions [e.g., *Duck et al.*, 2000] result in the downward control at 78°N being very different from that at midlatitudes and tropical latitudes. Indeed, lags similar to that reported here have been observed much earlier, for example, by *Reid and Gage* [1985] wherein sea surface temperature anomaly precedes the tropopause response by 2 months. Obviously there is no direct analogy here, but the existence of a persistent boundary layer inversion in winter effectively decoupling (in terms of temperature structure) the middle troposphere from very low surface temperatures constitutes a case somewhat special to very high latitude locations. Such inversions can often be seen in the temperature profiles (mentioned earlier) obtained from the micro pulse lidar at Ny Ålesund (approximately 90 km to the NW of the radar).

[18] Further investigation, a deeper excursion into meteorology, is beyond the scope of this paper and is left for future work: the goal of this study has been to document the refurbished SOUSY radar, SSR2, and further to present a novel approach to automatic radar tropopause height determination employing analysis of radar echo power.

#### 4. Conclusions

[19] It is clear that the SSR2 radar, even with its very modest peak power of only 1 kW, though still about 30 dB antenna gain, is easily capable of detecting echoes from the tropopause. We have presented a method of processing these echoes automatically in order to obtain time series of the radar-tropopause altitude. The seasonal variation agrees well with earlier measurements, simultaneous radiosonde measurements, and also with the *WMO* [1996] prediction. These seasonal variations (from the old SSR1 and new SSR2 SOUSY systems) lag approximately 1 month behind the corresponding surface temperature variations suggesting the importance of downward

---

**Figure 6.** (top) Height difference between monthly averages of the radar tropopause determined by SSR2 and the meteorological tropopause determined by radiosonde soundings from Ny Ålesund. (bottom) Scatterplot of radar tropopause determined by SSR2 and the meteorological tropopause determined by radiosonde, together with linear fit.

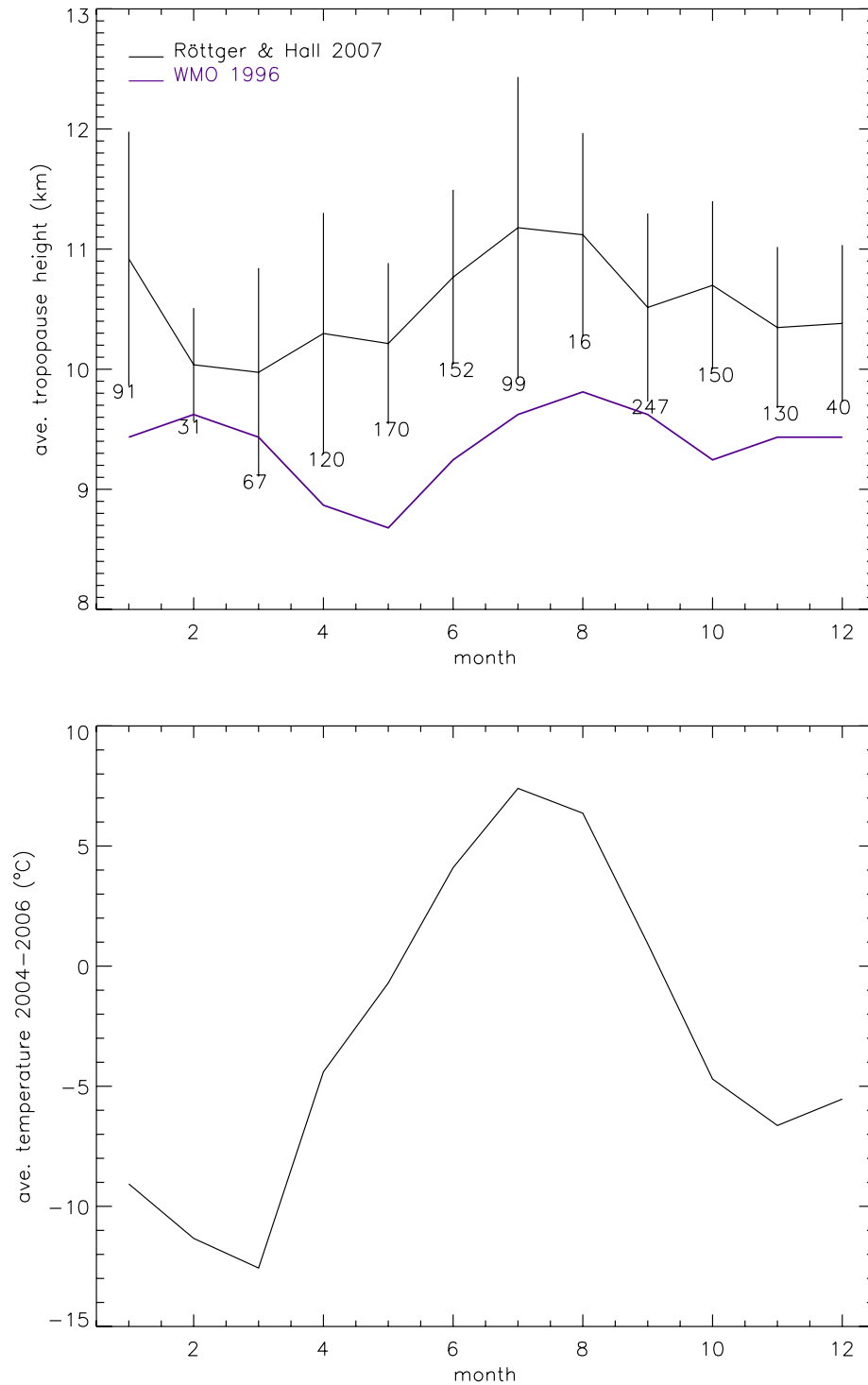


**Figure 7.** (top) Earlier results from *Röttger and Hall* [2007] using the SSR1 radar at the same location. The tropopause was identified by manual digitization, and the number of values (heights) per month is indicated by the numbers on the standard deviation bars. (bottom) Monthly average temperatures for the years 2004–2006 from Longyearbyen airport (courtesy of the Norwegian Meteorological Institute).

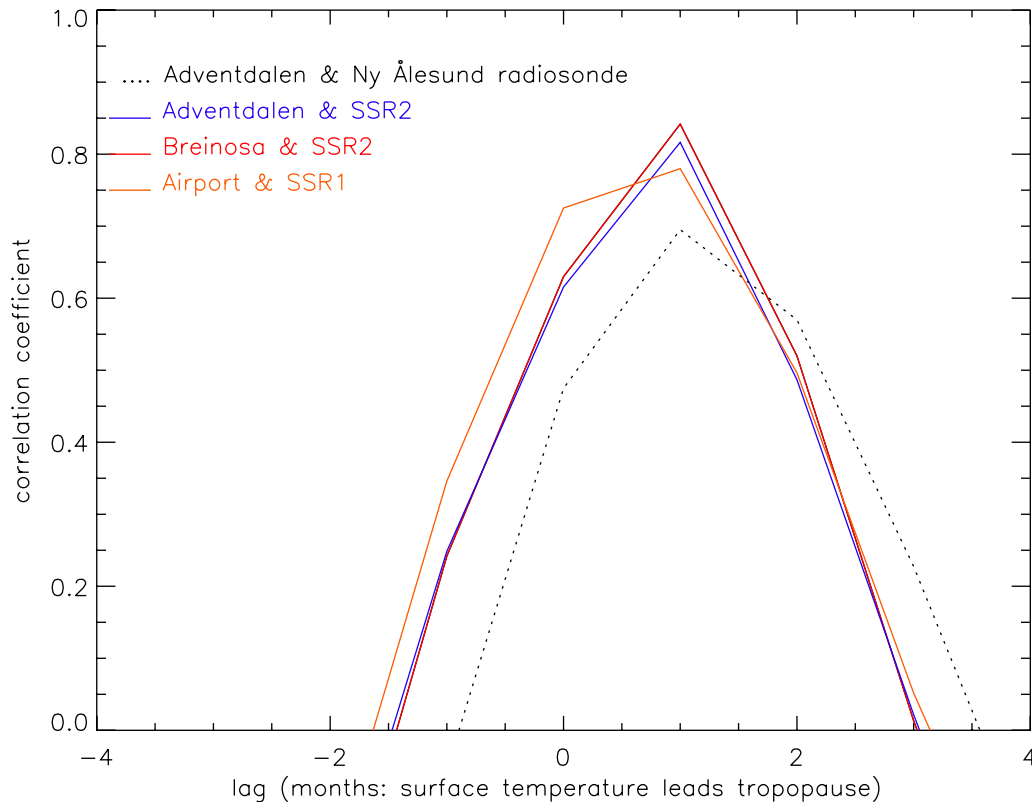


**Figure 8.** Correlation coefficient versus lag for: (1) Adventdalen valley floor and meteorological tropopause above Ny Ålesund (same coverage as SSR2), (2) Breinosa and SSR2 (2008 data) (narrowest), (3) Adventdalen valley floor and SSR2 (2008 data), and (4) temperature measured at Longyearbyen airport (widest) and “old” SOUSY system (2004–2006 data).

control from the stratosphere, combined with the possibility that, in winter at high latitude in particular, surface air temperature (i.e., the temperature near to the ground in a few meters height) poorly represents potential temperature in the troposphere. Further physical explanation of this lag is beyond the intended scope of this study (although it is discussed somewhat in the preceding section); however that the relationships between two (2004–2006 and 2007–2008) seasonal variations of tropopause height and four seasonal surface temperature in the close vicinity of the radar, five quite independent data sets, are consistent gives considerable faith in both instrument and algorithm.

[20] **Acknowledgments.** The authors are indebted to the Norwegian Amundsen Centre for economic support for the SSR2 radar. The authors would like express gratitude for the help and support of the Jicamarca staff, in particular the members of the Electronics and Instrumentation group and Victor Quesada. The NASA Micro-Pulse Lidar Network is funded by the NASA Earth Observing System and Radiation Sciences Program, and we thank Masataka Shiobara and staff at the National Institute of

Polar Research (Japan) for data from Ny Ålesund. We are indebted to the Alfred Wegener Institute, in particular Marion Maturilli, for tropopause data from their Ny Ålesund station. We also acknowledge the occasional maintenance of the SSR by the staff of the EISCAT Svalbard Radar.

## References

- Andrews, D. G., J. R. Holton, and C. B. Leovy (1987), *Middle Atmosphere Dynamics*, 489 pp., Academic, San Diego, Calif.
- Angell, J. K., and J. Korshover (1964), Quasi-biennial variations in temperature, total ozone and tropopause height, *J. Atmos. Sci.*, *21*, 479–492, doi:10.1175/1520-0469(1964)021<0479:QBVITT>2.0.CO;2.
- Duck, T. J., J. A. Whiteway, and A. L. Carswell (2000), A detailed record of high arctic middle atmospheric temperatures, *J. Geophys. Res.*, *105*(D18), 22,909–22,918, doi:10.1029/2000JD900367.
- Gage, K. S., and J. L. Green (1979), Tropopause detection by partial specular reflection with very-high-frequency radar, *Science*, *203*, 1238–1240, doi:10.1126/science.203.4386.1238.

- Gage, K. S., and J. L. Green (1982), An objective method for the determination of tropopause height from VHF radar observations, *J. Appl. Meteorol.*, *21*, 1150–1154.
- Hildebrand, P. H., and R. S. Sekhon (1974), Objective determination of the noise level in Doppler spectra, *J. Appl. Meteorol.*, *13*, 808–811, doi:10.1175/1520-0450(1974)013<0808:ODOTNL>2.0.CO;2.
- Hooper, D. A., and J. Arvelius (2000), Monitoring of the Arctic winter tropopause: A comparison of radiosonde, ozonesonde and MST radar observations, paper presented at MST-9 Workshop, Boulder, Colo.
- Jackway, P. T. (2000), Improved morphological top-hat, *Electron. Lett.*, *36*, 1194–1195, doi:10.1049/el:20000873.
- Reid, G. C., and K. S. Gage (1981), On the annual variation in height of the tropical tropopause, *J. Atmos. Sci.*, *38*, 1928–1938, doi:10.1175/1520-0469(1981)038<1928:OTAVIH>2.0.CO;2.
- Reid, G. C., and K. S. Gage (1985), Interannual variations in the height of the tropical tropopause, *J. Geophys. Res.*, *90*, 5629–5635, doi:10.1029/JD090iD03p05629.
- Röttger, J. (2000), Investigations of the mesosphere, stratosphere and the troposphere in Svalbard, *Adv. Polar Upper Atmos.*, *14*, 202–220.
- Röttger, J. (2001a), Observations of the Arctic troposphere and lower stratosphere with the SOUSY Svalbard radar, in *Environmental Research in the Arctic, Mem. Natl. Inst. Polar Res.*, *4*, 1–8.
- Röttger, J. (2001b), Observations of the polar D-region and the mesosphere with the EISCAT Svalbard radar and the SOUSY Svalbard radar, in *Environmental Research in the Arctic, Mem. Natl. Inst. Polar Res.*, *4*, 9–20.
- Röttger, J., and C. M. Hall (2007), Climatology of the radar tropopause over Svalbard 2005 and 2006, paper presented at MST-11 Workshop, India.
- Salby, M. L. (1996), *Fundamentals of Atmospheric Physics*, 627 pp., Academic, San Diego, Calif.
- Spearman, C. (1904), The proof and measurement of association between two things, *Am. J. Psychol.*, *15*, 72–101, doi:10.2307/1412159.
- World Meteorological Organization (WMO) (1996), Measurements of upper air temperature, pressure, and humidity, in *Guide to Meteorological Instruments and Methods of Observation*, 6th ed., *WMO I.12-1-I.12-32*, Geneva.
- 
- J. Chau and K. Kuyeng, Radio Observatorio de Jicamarca, Instituto Geofísico del Perú, Lima 13, Perú.
- S. Claes and F. Sigernes, University Centre in Svalbard, N-9171 Longyearbyen, Norway.
- C. M. Hall, Tromsø Geophysical Observatory, University of Tromsø, N-9037 Tromsø, Norway. (chris.hall@uit.no)
- J. Röttger, Max Planck Institute, D-37191 Katlenburg-Lindau, Germany.